DOI: 10.1002/ejic.200900308

Synthesis of Zinc Glycerolate Microstacks from a ZnO Nanorod Sacrificial Template

Róbert Rémiás,[a] Ákos Kukovecz,*[a] Mária Darányi,[a] Gábor Kozma,[a] Szilvia Varga,[a] Zoltán Kónya,[a] and Imre Kiricsi[a]

Keywords: Electron microscopy / Zinc / Nanostructures / Chelates / Sacrificial templating

We synthesized zinc glycerolate (ZnGly) microstacks by treating ZnO with glycerol at 100 °C under reflux. We observed that the morphology of the ZnO source has a pronounced effect on the appearance of the ZnGly product. In the absence of structure-directing effects the product ZnGly is obtained as a random heap of hexagonal prisms with an average diameter and thickness of ca. 2.5 μm and ca. 350 nm, respectively. However, bundles of nanorod-shaped ZnO obtained by the thermal decomposition of zinc oxalate nanorods could readily be transformed into 2–4 μm long zinc glycerolate microstacks in which 6–12 hexagonal prisms are aligned face-to-face. We present evidence that the ZnGly plates in the microstacks are bound together by forces strong enough to withstand mechanical deformation exercised by a contacting AFM tip. The ZnGly microstacks appear to emerge from the ZnO nanorod bundles in an approx. 1:1 ratio in the reactive template synthesis.

Introduction

Cosmetic and dermatological applications of nanotechnology have attracted considerable attention recently.[1] In fact, the pharmaceutical and the cosmetics industry are among the largest commercial benefactors of nanotechnology today.[2] Advances related to personal care products as well as therapeutic materials including novel nanosized carriers[3,4] or metallic[5,6] and semiconducting[7] nanoparticles, polymers[8] and magnetic materials[9] as active components appear with increasing frequency. The last few years have also seen an increased awareness[10] of the potential health hazards of nanomaterials,[8,11,12] their toxicity[13–15] and the necessity to study their interaction with living tissue in detail.[16,17] However, studies focused on controlling the morphology of health-agent nanoparticles are not evenly distributed among the potential materials, even though such advances could certainly contribute to the success of the emerging nano-cosmetology and nano-dermatology disciplines.

Zinc glycerolate (ZnGly) is a typical example of such a material. It is a slow-release nontoxic source of therapeutic zinc[18] with antiarthritic,[19] antiulcer,[20] and antiinflammatory[21] activity. Recently, Heideman et al. have reported on the applicability of ZnGly for replacing ZnO in various rubber compounds.[22] The general public is regularly exposed to ZnGly as it is effective against oral herpetic sores[23] and serves as the active component of the product "GlyZinc." It belongs to the monoclinic crystal system, space group $P2_1/c$ and exhibits a strong tendency towards forming platelike hexagonal crystals with a prismatic habit.[24] Until now, no attempt was made to direct the growth of zinc glycerolate into any morphology other than a random assembly of hexagonal prisms. It should be noted though that Moleski et al. have recently succeeded in the controlled conversion of ZnGly into ZnO nanoparticles.[25]

Zinc, cobalt, manganese, and iron monoglycerolates all have a similar structure and can be synthesized by using the same reaction.[26–29] Cobalt glycerolate appears to be particularly important today as it is a layered antiferromagnetic material, which was recently shown by Pratt et al.[30] to exhibit a chiral-like critical behavior. Nontransition-metal glycerolates like calcium glycerolate[31] and lead glycerolate[32] have also attracted some attention in the past. Gaining more control over the nanoscale morphology of zinc glycerolate is expected to advance the evolution of these related fields as well.

Bottom-up methods are used extensively for the synthesis of several nanostructured materials including for example biological nanomaterials,[33] self-assembled monolayers,[34] and nanoelectronics components.[35] Their common advantage is that they exploit the natural shape and pattern formation drive of materials and therefore, they are generally cheaper and more scalable then top-down approaches. On the other hand, the lack of a suitable structure-directing agent or template can hinder the development of a bottom-

[a] Department of Applied and Environmental Chemistry, University of Szeged,
Rerrih Béla tér 1, 6720 Szeged, Hungary
Fax: +36-62-544-619
E-mail: kakos@chem.u-szeged.hu

Supporting information for this article is available on the WWW under http://dx.doi.org/10.1002/ejic.200900308.

up method considerably. Ideally, the morphology of the reactants should be mirrored in the structure of the product to give the most feasible bottom-up synthesis. In some reaction types (e.g. calcination of oxalate precursors[36] or the conversion of titanate nanowires into anatase nanowires[36]) this is readily achieved, whereas other reactions – especially the ones involving the complete chemical restructuring of both reactants – are generally not available for reactive templating.[37]

In the present contribution we give a working example for a complete bottom-up synthesis with sacrificial templating: first, we exploit a natural pattern formation tendency of nonstructured starting materials to obtain zinc oxalate nanorods, then we use a well-known reactive templating reaction to transform these into ZnO nanorods, and finally, we copy the rodlike structure of ZnO into a completely different material, zinc glycerolate by sacrificial templating.

Results and Discussion

In Figure 1 we present the XRD profiles of the materials discussed. The characteristic wurtzite ZnO reflections indexed in curve (a) are present both in the diffractogram of the commercial ZnO source (a) and the profile of the nanorods (b) synthesized according to Ha et al.[38] For reference, the profile of the zinc oxalate intermediate is also shown as curve (c) and indexed on a basis of a monoclinic cell of zinc oxalate dihydrate. Profiles (d) and (e) are characteristic of zinc glycerolate synthesized from commercial ZnO powder and ZnO nanorods, respectively. The signature reflections of zinc glycerolate are found at 11.1° (100), 17.2° (011), 20.7° (111), 23.8° (102), 24.8° (012), and 27.6° (020) with several minor peaks in the 28–50° range. It can be seen that (i) both ZnO sources could be transformed into zinc glycerolate, and (ii) zinc glycerolate synthesized from ZnO nanorods appears to contain less ZnO impurities than its commercial ZnO-based counterpart.

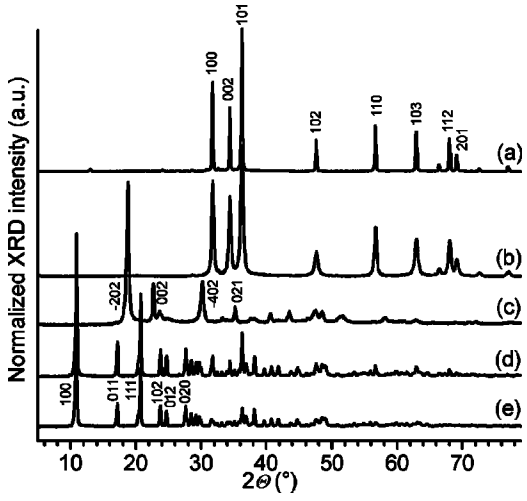

Figure 1. XRD profiles of commercial ZnO powder (a), ZnO nanorods (b) prepared from zinc oxalate nanorods (c), unaligned zinc glycerolate prepared from commercial ZnO powder (d), and zinc glycerolate microstacks prepared from ZnO nanorods (e).

The morphology of the ZnO nanorods can be assessed in Figure 2. Individual zinc oxalate nanorods (Figure 2a) are typically over 1 μm long and measure less than 100 nm in diameter. They are organized into bundles over 3 μm long and over 500 nm in diameter. This structure is mirrored in the ZnO nanorods (Figure 2b) prepared from zinc oxalate. Here the individual rods are close to 2 μm in length and less than 100 nm in diameter, whereas the ZnO bundles (microrods) are longer than 3 μm, and their diameter is approx. 500 nm. Thus, the morphology of the synthesized rodlike ZnO agrees well with results published earlier[38,39] and demonstrates the success of the first reactive templating step. In Figure 2c the morphology of the commercial ZnO powder used as a reference is shown. The ZnO particles have a broad diameter distribution with a mean particle size of 1100 nm and random particle alignment.

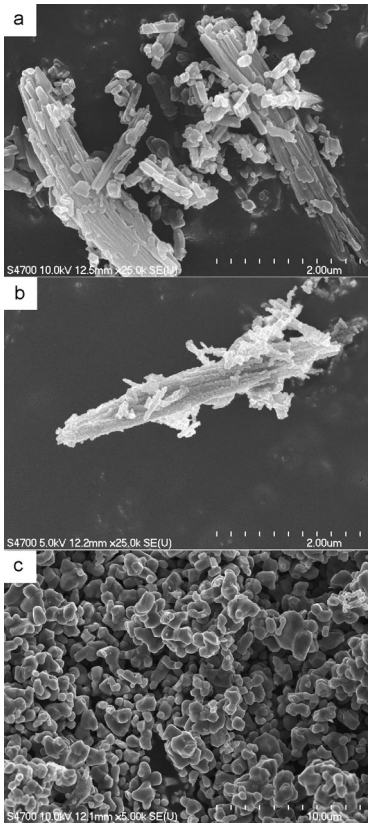

Figure 2. SEM images of hydrothermally synthesized zinc oxalate nanorods (a), ZnO nanorods obtained from these by calcination (b), and a reference commercial ZnO powder (c).

Zinc glycerolate synthesized from this commercial ZnO powder (Figure 3a) consists of a random assembly of hexagonal crystals averaging ca. 2.5 μm in diameter and ca. 350 nm in thickness. Since no structure-directing effects were at work in the reaction mixture, there is no preferential crystal-face alignment. This finding is in agreement with the work of Hambley and Snow[24] who did not note any orientation effects in ZnGly prepared from commercial ZnO. In Figure 3b we present the image of the same material after sonicating it in ethanol in a low-energy ultrasonic bath for 20 min and then allowing the suspension to settle

gently without mechanical disturbances. This experiment was performed in order to loosen up the zinc glycerolate crystals and see if stacking interactions alone could re-assemble the hexagonal platelets on top of each other. Figure 3b clearly proves this hypothesis void: the alignment of the crystals remained random after sonication. Therefore, we may conclude that spontaneous stacking forces acting between the zinc glycerolate crystals are inadequate to exercise any orientation effect on the material.

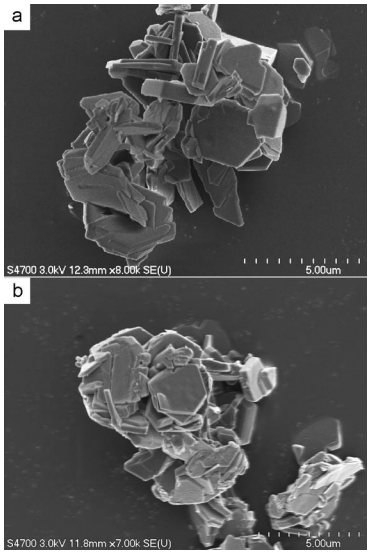

Figure 3. SEM images of zinc glycerolate as-synthesized from commercial ZnO powder (a) and the same material after being sonicated for 20 min and allowed to settle down (b).

Zinc glycerolate prepared from ZnO microrods consists of hexagonal crystals with a mean diameter and thickness of ca. 1400 nm and ca, 330 nm, respectively (Figure 4a). However, the particles are well oriented in this case. Alignment is ensured by the stacking basal planes of the hexagonal prisms and results in an irregularly shaped ZnGly microstack with a long axis perpendicular to the crystallographic *bc* plane of the crystals. Typically, one microstack consists of 6–12 zinc glycerolate prisms and has a total length of 2–4 μm (Figure 4b, c). The excellent match between the XRD profiles of the randomly aligned zinc glycerolate phase and the microstacks (Figure 1) indicates that their crystal structures are identical.

Infrared spectra (Figure 5) were recorded to assess the similarity on the molecular scale. Spectra (a) and (b) belong to the randomly oriented and the microstack-structured ZnGly, respectively. Curve (c) is the reference spectrum of glycerol. The characteristic ν(O–H), ν(C–H), and (νC–O) vibrations of glycerol are observable at 3360, 2910, 1124, and 1046 cm^{-1}.[40] The narrowing of the glycerol bands in ZnGly is due to the crystalline nature of the material. The formation of the zinc glycerolate phase is indicated by the shifting of certain glycerol bands (e.g. from 676 cm^{-1} in glycerol to 653 cm^{-1} in ZnGly and from 1046 cm^{-1} in glycerol to 1065 cm^{-1} in ZnGly) and the appearance of the bands at 2500 cm^{-1} and 1940 cm^{-1}. These can be assigned to OH stretching and CO stretching vibrations where the

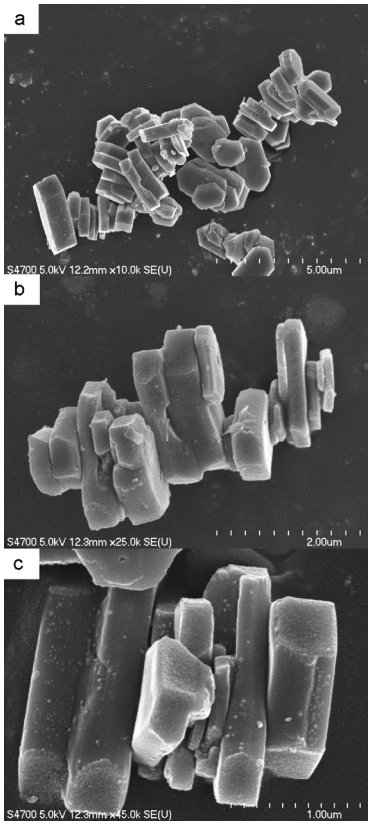

Figure 4. Typical SEM images of zinc glycerolate microstacks.

oxygen atom is involved in an O–H···O hydrogen bond, respectively. Spectral changes all originate from the confinement of the glycerato ligands into well-defined 5-membering structures in the zinc glycerolate chelate compound as described in the original report of Radoslovich et al.[41] The spectra of the two ZnGly phases – curves (a) and (b) – are almost identical; therefore, the structure of the randomly aligned material and the microstacks can be considered the same on the molecular level as well.

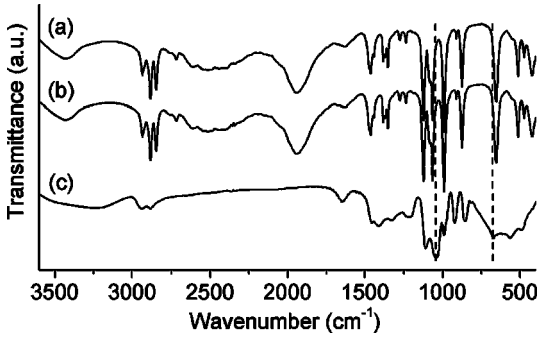

Figure 5. Infrared spectra of zinc glycerolate prepared from commercial ZnO powder (a) and zinc glycerolate microstacks (b). The spectrum of liquid glycerol is shown in curve (c) as a reference.

A close-up view of the prism–prism interface (Figure 4c) in the microstacks suggests that 3–5 prisms may be grown together because even at high magnification no gap is vis-

ible between them. However, it is not possible to decide on the basis of the SEM images alone if this really is the case or if the ZnGly prisms are merely stacking together.

In Figure 6 an AFM image of the zinc glycerolate microstacks is presented. Letters A–E mark five different ZnGly microstack examples, and several more unmarked ones are also visible. The physical dimensions and the stacked hexagonal-prism structure of the microstacks determined from the AFM measurement agree well with the SEM observations. In order to test the validity of the assumption that the ZnGly hexagons are attached to each other, we lowered the AFM probe to the top left corner of the ZnGly assembly marked F and moved the tip back and forth 2 μm in the sample plane. This method is based on the work of Biro et al. who used a similar technique to prove the presence of chemical linkage between functionalized carbon nanotubes by STM.[42] The image on the right-hand side in Figure 6 depicts the studied area after the manipulation. The damage caused by the AFM tip to the ZnGly object F is observable as a white spot. Moreover, it is also visible that the F assembly has flipped over the top left/bottom right diagonal of the image. Since neither the A–E microstacks nor the unmarked ZnGly units changed their relative positions, the movement of F can only be assigned to the agitation effect of the tip. Let us now observe that object F consisted of two hexagonal prisms originally. This structure is completely preserved: both prisms appear to have moved together, without changing their relative position even though the force exercised by the AFM tip was large enough to damage the ZnGly crystal itself. This finding complements the SEM results (Figure 4c) and suggests that the hexagonal ZnGly prisms in one microstack not only appear to be very close but they are indeed bound together. It is not yet possible to determine if this is through a primary chemical bond (that is, ZnGly prisms grown together) or van der Waals forces, but the attachment is certainly strong enough to preserve the microstack structure even when subjected to a considerable deformation force. Further studies are required to uncover the exact role of the noncrystalline material visible (Figure 4c) between the individual ZnGly prisms in the structural integrity of the microstacks.

The most peculiar finding of our work is that ZnO nanorod bundles can serve as sacrificial templates and give an organometallic reaction product. This is the inverse of the more common path of converting a shape-controlled hydroxide[43,44] or organic salt[39,45] into an oxide nanorod. Examples of similar conversions are scarcely found in the literature. Besides the mentioned oxide production reactions, reactive templating is mostly used for the preparation of low-dimensional electroceramic nanostructures[46–48] today.

Concerning the mechanism of the zinc glycerolate microstack formation it seems evident that the ZnO microrod can not dissolve fully in the first reaction step because in that case the structure-directing phenomenon would not be observable. It is also clear that ZnO microrods are consumed in the reaction, which makes the synthesis a working example of a reactive templating bottom-up method. However, it is an open question if the ZnO → ZnGly conversion progresses from one end of the ZnO rod to the other or takes place along the whole length simultaneously. It has been reported earlier that the ZnO surface can interact with –OH groups through hydrogen bonds[49] and that different ZnO facets exhibit different affinities towards interaction with polyethylene glycol.[50] Combining these findings with our experience in diffusion-limited hydrothermal growth in static autoclaves we suggest that the former option has a higher probability.[51]

That is, the end of the ZnO microrod is more likely to be attacked by the chelating agent glycerol. Since the autoclave is not agitated, the volume near the end of the nanorod could become locally oversaturated for zinc glycerolate, which will spontaneously crystallize in hexagonal prisms. The close proximity (there is no convection in the system because the autoclave is static) of the previously formed ZnGly prisms will then allow the system to minimize its surface energy by the attachment of the prisms to a ZnGly microstack (Figure 7). A similar explanation has recently been offered to explain the formation of ZnO doughnuts by Ghoshal et al.[52] On the other hand, when the synthesis is done from randomly oriented commercial ZnO particles the ZnGly prisms are not aligned well enough to allow proximity-induced surface-energy minimalization (Figure 3), and therefore ZnGly microstack formation does not take place.

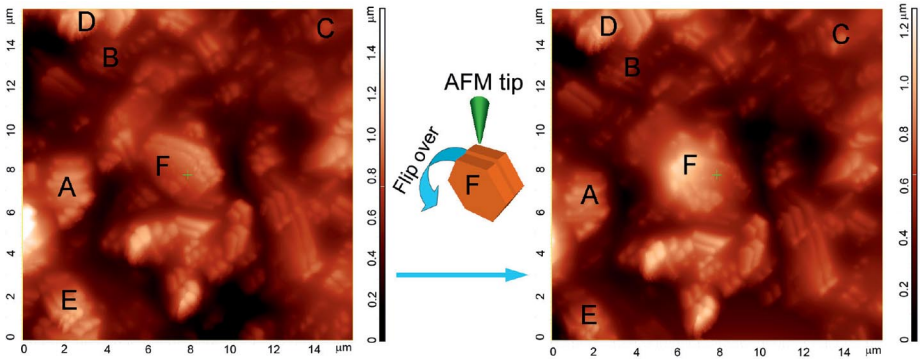

Figure 6. AFM images of zinc glycerolate microstacks before (left) and after (right) flipping the hexagonal prism assembly "F" over by an AFM tip. Positions A–E mark some typical ZnGly microstacks unaffected by the AFM manipulation.

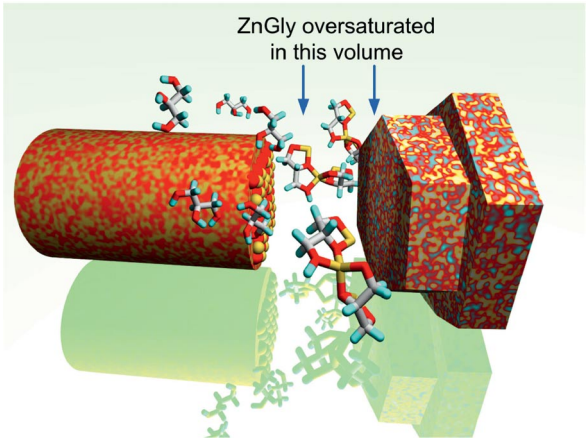

Figure 7. Illustration of the conversion of a ZnO nanorod bundle (on the left) into a ZnGly microstack (on the right) upon the attack of chelating agent glycerol. When the same reaction takes place in an agitated vessel, the ZnGly hexagonal prisms cannot attach to each other to form a microstack.

The diameter difference between the ZnO microrods and the ZnGly microstacks could be related to the different structure (wurtzite crystal vs. chelato complex) of the materials. Whereas the density of wurtzite ZnO[53] is 5.6 g cm^{-3}, the density of zinc glycerolate is 2.2 g cm^{-3} according to Hambley and Snow.[24] This ca. 250% density difference matches the observed mean diameter difference (ca. 500 nm for a ZnO nanorod bundle vs. ca. 1400 nm for a ZnGly microstack, see Figures 2 and 4) well. Combined with the fact that the mean length of a ZnO nanorod bundle and that of a ZnGly microstack are similar we may assume that on average, one ZnO nanorod bundle is converted into one ZnGly microstack during the hydrothermal treatment. The reason for the heterogeneous size distribution of the ZnGly prisms within one microstack is still unclear; one may hypothesize that it is related to the nonuniform cross-section (Figure 2b) of the ZnO nanorods or to local concentration fluctuation effects.

Conclusions

We synthesized zinc glycerolate (ZnGly) by treating ZnO with glycerol. We observed that the morphology of the ZnO source has a large effect on the appearance of the ZnGly product. In the absence of structure-directing effects the product ZnGly is obtained as a random heap of hexagonal prisms. Their alignment remains random even if subjected to ultrasonic perturbation and subsequent relaxation. However, nanorod-shaped ZnO could readily be transformed into zinc glycerolate microstacks in which 6–12 hexagonal prisms are aligned face-to-face. We presented evidence that the ZnGly plates in the microstacks are bound together by forces strong enough to withstand mechanical deformation exercised by a contacting AFM tip and suggested a formation scheme to explain the main features of the ZnO microrod to ZnGly microstack conversion.

We suggest that the glycerolate microstack preparation principle reported here could easily be extended to cover the preparation of microstacks from other glycerolate-forming metal oxide nanorods, e.g. iron, cobalt, and manganese oxides. Although some questions concerning the exact formation mechanism of ZnGly microstacks are still open, we expect that with the expansion of the nano-dermatology field and the recent interest in layered magnetic materials, answers will come soon.

Experimental Section

Synthesis of ZnO Nanorods: $Zn(NO_3)_2 \cdot 6H_2O$ (10 mmol, Reachim) and oxalic acid (10 mmol) were dissolved in absolute ethanol (40–40 mL, Molar) and mixed together thoroughly at room temperature. The resulting mixture was transferred into a Teflon-lined stainless steel autoclave and kept at 130 °C for 10 h. The product mixture was filtered, washed with distilled water and ethanol, and dried at 80 °C in air overnight. Finally, the synthesized zinc oxalate was decomposed to ZnO by calcination at 420 °C in an N_2 flow for 2 h (heating temperature ramp was set to 2.5 °C min^{-1}).

Synthesis of Zinc Glycerolate (ZnGly): ZnO (0.25 g, either a commercial product from Reanal or the nanorods described above) was mixed with glycerol (25 mL, Molar) at 100 °C under reflux for 4 h. The resulting mixture was transferred into a Teflon-lined stainless steel autoclave and kept at 150 °C for 24 h. The product mixture was filtered, washed with distilled water, and dried at 80 °C in air overnight.

Characterization: X-ray diffraction profiles were recorded with a Rigaku Miniflex 2 instrument by using Cu-K_α radiation. Scanning electron microscopy (SEM) was performed with a Hitachi S-4700 Type II cold field-emission microscope. Samples were sputter-coated by an approx. 5 nm thick Au/Pd layer before measurement to avoid charging effects. Infrared (IR) spectra were recorded in a KBr matrix with a Bruker Vertex 70 FT-IR instrument under ambient conditions averaging 64 scans at a resolution of 4 cm^{-1}. Atomic force microscopy images were recorded with an NT-MDT Smena A unit on HOPG substrate in semi-contact mode by using TAP300GD tips with a resonance frequency of 300 kHz and force constant 40 N/m.

Supporting Information (see footnote on the first page of this article): Reverse scan direction image of Figure 6.

Acknowledgments

The financial support of the Hungarian Scientific Research Fund (OTKA) through projects NNF-78920 and 73676 is acknowledged.

[1] S. J. Choi, J. M. Oh, J. H. Choy, *J. Mater. Chem.* **2008**, *18*, 615–620.
[2] M. Goldberg, R. Langer, X. Q. Jia, *J. Biomater. Sci., Polym. Ed.* **2007**, *18*, 241–268.
[3] R. H. Muller, M. Radtke, S. A. Wissing, *Adv. Drug Delivery Rev.* **2002**, *54*, S131–S155.
[4] R. H. Muller, R. D. Petersen, A. Hornmoss, J. Pardeike, *Adv. Drug Delivery Rev.* **2007**, *59*, 522–530.
[5] K. C. Bhol, P. J. Schechter, *Br. J. Dermatol.* **2005**, *152*, 1235–1242.
[6] L. S. Nair, C. T. Laurencin, *J. Biomed. Nanotechnol.* **2007**, *3*, 301–316.

[7] T. Maier, H. C. Korting, *Skin. Pharmacol. Physiol.* **2005**, *18*, 253–262.
[8] P. Somasundaran, S. Chakraborty, Q. Qiang, P. Deo, J. Wang, R. Zhang, *J. Cosmet. Sci.* **2004**, *55*, S1–S17.
[9] I. Perelshtein, N. Perkas, S. Magdassi, T. Zioni, M. Royz, Z. Maor, A. Gedanken, *J. Nanopart. Res.* **2008**, *10*, 191–195.
[10] O. Renn, M. C. Roco, *J. Nanopart. Res.* **2006**, *8*, 153–191.
[11] G. J. Nohynek, J. Lademann, C. Ribaud, M. S. Roberts, *Crit. Rev. Toxicol.* **2007**, *37*, 251–277.
[12] R. Brayner, *Nano Today* **2008**, *3*, 48–55.
[13] J. W. Seo, A. Magrez, M. Milas, K. Lee, V. Lukovac, L. Forro, *J. Phys. D: Appl. Phys.* **2007**, *40*, R109–R120.
[14] A. Magrez, S. Kasas, V. Salicio, N. Pasquier, J. W. Seo, M. Celio, S. Catsicas, B. Schwaller, L. Forro, *Nano Lett.* **2006**, *6*, 1121–1125.
[15] A. Nel, T. Xia, L. Madler, N. Li, *Science* **2006**, *311*, 622–627.
[16] G. Jia, H. F. Wang, L. Yan, X. Wang, R. J. Pei, T. Yan, Y. L. Zhao, X. B. Guo, *Environ. Sci. Technol.* **2005**, *39*, 1378–1383.
[17] C. Kirchner, T. Liedl, S. Kudera, T. Pellegrino, A. M. Javier, H. E. Gaub, S. Stolzle, N. Fertig, W. J. Parak, *Nano Lett.* **2005**, *5*, 331–338.
[18] D. P. Fairlie, M. W. Whitehouse, R. M. Taylor, *Agents Actions.* **1992**, *36*, 152–158.
[19] M. W. Whitehouse, K. D. Rainsford, R. M. Taylor, B. Vernon-roberts, *Agents Actions.* **1990**, *31*, 47–58.
[20] K. D. Rainsford, M. W. Whitehouse, *J. Pharm. Pharmacol.* **1992**, *44*, 476–482.
[21] M. W. Whitehouse, D. P. Fairlie, Y. H. Thong, *Agents Actions.* **1994**, *42*, 123–127.
[22] G. Heideman, J. W. M. Noordermeer, R. N. Datta, *KGK, Kautsch. Gummi Kunstst.* **2006**, *59*, 178–183.
[23] A. Apisariyakulm, D. Buddhasukh, S. Apisariyakul, B. Ternai, *Med. J. Aust.* **1990**, *152*, 54–54.
[24] T. W. Hambley, M. R. Snow, *Aust. J. Chem.* **1983**, *36*, 1249–1253.
[25] R. Moleski, E. Leontidis, F. Krumeich, *J. Colloid Interface Sci.* **2006**, *302*, 246–253.
[26] L. Rodrique, G. Delvaux, A. Dardenne, *Powder Technol.* **1978**, *19*, 93–101.
[27] P. Bruylants, A. Munaut, G. Poncelet, J. Ladriere, J. Meyers, J. Fripiat, *J. Inorg. Nucl. Chem.* **1980**, *42*, 1603–1611.
[28] E. Mendelovici, A. Sagarzazu, R. Villalba, *J. Therm. Anal.* **1993**, *40*, 1115–1122.
[29] E. Mendelovici, R. Villalba, A. Sagarzazu, *J. Mater. Sci. Lett.* **1990**, *9*, 28–31.
[30] F. L. Pratt, P. J. Baker, S. J. Blundell, T. Lancaster, M. A. Green, M. Kurmoo, *Phys. Rev. Lett.* **2007**, *99*, 017202.
[31] R. M. Taylor, P. G. Slade, G. L. Aldous, I. R. Wilding, O. Siddiqui, M. W. Whitehouse, *Aust. J. Chem.* **1992**, *45*, 1179–1185.
[32] H. L. Keller, H. J. Riebe, *Z. Anorg. Allg. Chem.* **1987**, *550*, 102–108.
[33] S. W. Lee, W. J. Chang, R. Bashir, Y. M. Koo, *Biotechnol. Bioprocess Eng.* **2007**, *12*, 185–199.
[34] J. J. Gooding, F. Mearns, W. R. Yang, J. Q. Liu, *Electroanalysis* **2003**, *15*, 81–96.
[35] W. Lu, C. M. Lieber, *Nat. Mater.* **2007**, *6*, 841–850.
[36] J. Y. Fang, J. Wang, S. C. Ng, C. H. Chew, L. M. Gan, *Nanostruct. Mater.* **1997**, *8*, 499–505.
[37] G. Z. Cao, D. W. Liu, *Adv. Colloid Interface Sci.* **2008**, *136*, 45–64.
[38] Z. G. Ha, L. H. Yue, Y. F. Zheng, Z. D. Xu, *Mater. Chem. Phys.* **2008**, *107*, 137–141.
[39] T. Ahmad, S. Vaidya, N. Sarkar, S. Ghosh, A. K. Ganguli, *Nanotechnology* **2006**, *17*, 1236–1240.
[40] A. Mudalige, J. E. Pemberton, *Vib. Spectrosc.* **2007**, *45*, 27–35.
[41] E. W. Radoslovich, M. Raupach, P. G. Slade, R. M. Taylor, *Aust. J. Chem.* **1970**, *23*, 1963–1971.
[42] A. A. Koos, Z. E. Horvath, Z. Osvath, L. Tapaszto, K. Niesz, Z. Konya, I. Kiricsi, N. Grobert, M. Ruhle, L. P. Biro, *Mater. Sci. Eng., C* **2003**, *23*, 1007–1011.
[43] B. Liu, S. H. Yu, F. Zhang, L. J. Li, Q. Zhang, L. Ren, K. Jiang, *J. Phys. Chem. B* **2004**, *108*, 4338–4341.
[44] L. Yan, R. B. Yu, G. R. Liu, X. R. Xing, *Scr. Mater.* **2008**, *58*, 707–710.
[45] S. H. Yu, M. Yoshimura, *Adv. Mater.* **2002**, *14*, 296.
[46] T. Sato, Y. Yoshida, T. Kimura, *J. Am. Ceram. Soc.* **2007**, *90*, 3005–3008.
[47] Y. A. Chung, C. Y. Lee, C. W. Peng, H. T. Chiu, *Mater. Chem. Phys.* **2006**, *100*, 380–384.
[48] T. Kimura, *J. Ceram. Soc. Jpn.* **2006**, *114*, 15–25.
[49] S. Liufu, H. Xiao, Y. P. Li, *Powder Technol.* **2004**, *145*, 20–24.
[50] X. M. Liu, Y. C. Zhou, *J. Cryst. Growth* **2004**, *270*, 527–534.
[51] A. Kukovecz, N. Hodos, E. Horvath, G. Radnoczi, Z. Konya, I. Kiricsi, *J. Phys. Chem. B* **2005**, *109*, 17781–17783.
[52] T. Ghoshal, S. Kar, S. Chaudhuri, *Cryst. Growth Des.* **2007**, *7*, 136–141.
[53] D. R. Lide (Ed.), *CRC Handbook of Chemistry and Physics*, CRC Press, Boca Raton, FL, **2005**.

Received: April 2, 2009
Published Online: July 14, 2009

